We are IntechOpen, the world's leading publisher of Open Access books Built by scientists, for scientists

4,800
Open access books available

122,000
International authors and editors

135M
Downloads

Our authors are among the

154
Countries delivered to

TOP 1%
most cited scientists

12.2%
Contributors from top 500 universities

CLARIVATE ANALYTICS BOOK CITATION INDEX INDEXED

WEB OF SCIENCE™

Selection of our books indexed in the Book Citation Index in Web of Science™ Core Collection (BKCI)

Interested in publishing with us?
Contact book.department@intechopen.com

Numbers displayed above are based on latest data collected.
For more information visit www.intechopen.com

11

Robust Stabilization and Discretized PID Control

Yoshifumi Okuyama
Tottori University, Emeritus
Japan

1. Introduction

At present, almost all feedback control systems are realized using discretized (discrete-time and discrete-value, i.e., digital) signals. However, the analysis and design of discretized/quantized control systems has not been entirely elucidated. The first attempt to elucidate the problem was described in a paper by Kalman (1) in 1956. Since then, many researchers have studied this problem, particularly the aspect of understanding and mitigating the quantization effects in quantized feedback control, e.g.,(2–4). However, few results have been obtained for the stability analysis of the nonlinear discrete-time feedback system.

This article describes the robust stability analysis of discrete-time and discrete-value control systems and presents a method for designing (stabilizing) PID control for nonlinear discretized systems. The PID control scheme has been widely used in practice and theory thus far irrespective of whether it is continuous or discrete in time (5; 6) since it is a basic feedback control technique.

In the previous study (7–9), a robust stability condition for nonlinear discretized control systems that accompany discretizing units (quantizers) at equal spaces was examined in a frequency domain. It was assumed that the discretization is executed at the input and output sides of a nonlinear continuous elemet (sensor/actuator) and that the sampling period is chosen such that the size is suitable for discretization in the space. This paper presents a designing problem for discretized control systems on a grid pattern in the time and controller variables space. In this study, the concept of modified Nyquist and Nichols diagrams for nonlinear control systems given in (10; 11) is applied to the designing procedure in the frequency domain.

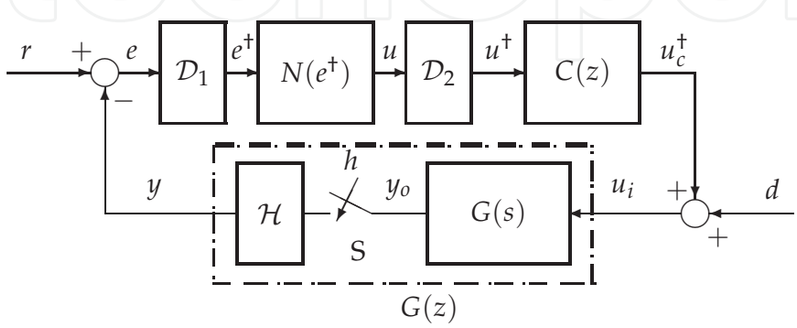

Fig. 1. Nonlinear discretized PID control system.

2. Discretized control system

The discretized control system in question is represented by a sampled-data (discrete-time) feedback system as shown in Fig. 1. In the figure, $G(z)$ is the z-transform of continuous plant $G(s)$ together with the zero-order hold, $C(z)$ is the z-transform of the digital PID controller, and $\mathcal{D}_1$ and $\mathcal{D}_2$ are the discretizing units at the input and output sides of the nonlinear element, respectively.

The relationship between e and $u^\dagger = N_d(e)$ is a stepwise nonlinear characteristic on an integer-grid pattern. Figure 2 (a) shows an example of discretized sigmoid-type nonlinear characteristic. For C-language expression, the input/output characteristic can be written as

$$\begin{aligned} e^\dagger &= \gamma * (\text{double})(\text{int})(e/\gamma) \\ u &= 0.4 * e^\dagger + 3.0 * \text{atan}(0.6 * e^\dagger) \\ u^\dagger &= \gamma * (\text{double})(\text{int})(u/\gamma), \end{aligned} \tag{1}$$

where (int) and (double) denote the conversion into an integral number (a round-down discretization) and the reconversion into a double-precision real number, respectively. Note that even if the continuous characteristic is linear, the input/output characterisitc becomes nonlinear on a grid pattern as shown in Fig. 2 (b), where the linear continuous characteristic is chosen as $u = 0.85 * e^\dagger$.

In this study, a round-down discretization, which is usually executed on a computer, is applied. Therefore, the relationship between $e^\dagger$ and $u^\dagger$ is indicated by small circles on the stepwise nonlinear characteristic. Here, each signal $e^\dagger$, $u^\dagger$, $\cdots$ can be assigned to an integer number as follows:

$$\begin{aligned} e^\dagger &\in \{\cdots, -3\gamma, -2\gamma, -\gamma, 0,\ \gamma,\ 2\gamma,\ 3\gamma, \cdots\}, \\ u^\dagger &\in \{\cdots, -3\gamma, -2\gamma, -\gamma, 0,\ \gamma,\ 2\gamma,\ 3\gamma, \cdots\}, \end{aligned}$$

where γ is the resolution of each variable. Without loss of generality, hereafter, it is assumed that $\gamma = 1.0$. That is, the variables $e^\dagger$, $u^\dagger$, $\cdots$ are defined by integers as follows:

$$e^\dagger, u^\dagger \in Z, \qquad Z = \{\cdots -3, -2, -1, 0, 1, 2, 3, \cdots\}.$$

On the other hand, the time variable t is given as $t \in \{0, h,\ 2h,\ 3h, \cdots\}$ for the sampling period h. When assuming $h = 1.0$, the following expression can be defined:

$$t \in Z_+, \quad Z_+ = \{0, 1, 2, 3, \cdots\}.$$

Therefore, each signal $e^\dagger(t)$, $u^\dagger(t)$, $\cdots$ traces on a grid pattern that is composed of integers in the time and controller variables space.

The discretized nonlinear characteristic

$$u^\dagger = N_d(e^\dagger) = K\, e^\dagger + g(e^\dagger), \qquad 0 < K < \infty, \tag{2}$$

as shown in Fig. 2(a) is partitioned into the following two sections:

$$|g(e^\dagger)| \le \bar{g} < \infty, \tag{3}$$

for $|e^\dagger| < \varepsilon$, and

$$|g(e^\dagger)| \le \beta\, |e^\dagger|, \qquad 0 \le \beta \le K, \tag{4}$$

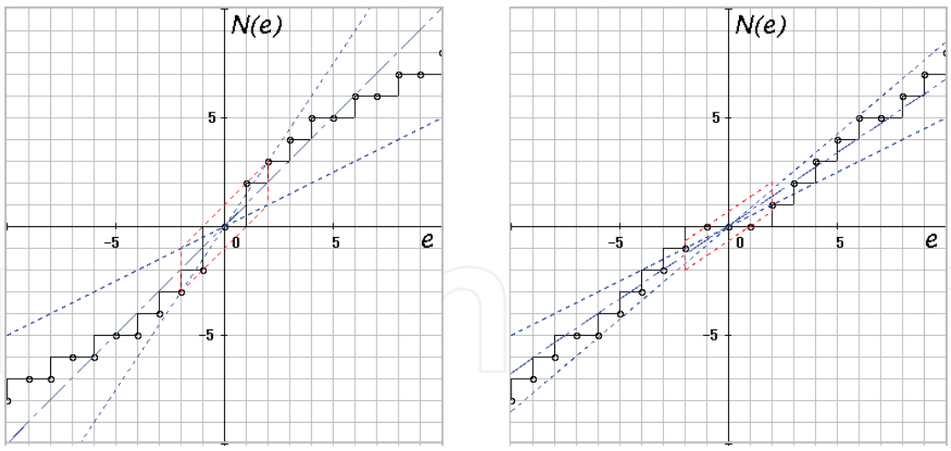

(a) (b)

Fig. 2. Discretized nonlinear characteristics on a grid pattern.

for $|e^{\dagger}| \geq \varepsilon$. (In Fig. 2 (a) and (b), the threshold is chosen as $\varepsilon = 2.0$.)
Equation (3) represents a bounded nonlinear characteristic that exists in a finite region. On the other hand, equation (4) represents a sectorial nonlinearity for which the equivalent linear gain exists in a limited range. It can also be expressed as follows:

$$0 \leq g(e^{\dagger})e^{\dagger} \leq \beta e^{\dagger 2} \leq K e^{\dagger 2}. \tag{5}$$

When considering the robust stability in a global sense, it is sufficient to consider the nonlinear term (4) for $|e^{\dagger}| \geq \varepsilon$ because the nonlinear term (3) can be treated as a disturbance signal. (In the stability problem, a fluctuation or an offset of error is assumed to be allowable in $|e^{\dagger}| < \varepsilon$.)

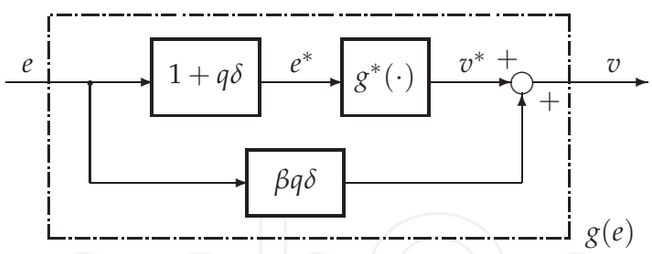

Fig. 3. Nonlinear subsystem $g(e)$.

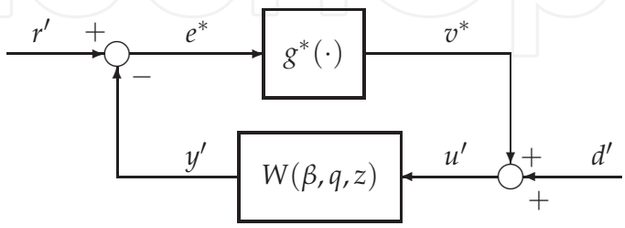

Fig. 4. Equivalent feedback system.

3. Equivalent discrete-time system

In this study, the following new sequences $e_m^{*\dagger}(k)$ and $v_m^{*\dagger}(k)$ are defined based on the above consideration:

$$e_m^{*\dagger}(k) = e_m^{\dagger}(k) + q \cdot \frac{\Delta e^{\dagger}(k)}{h}, \tag{6}$$

$$v_m^{*\dagger}(k) = v_m^{\dagger}(k) - \beta q \cdot \frac{\Delta e^{\dagger}(k)}{h}, \tag{7}$$

where q is a non-negative number, $e_m^{\dagger}(k)$ and $v_m^{\dagger}(k)$ are neutral points of sequences $e^{\dagger}(k)$ and $v^{\dagger}(k)$,

$$e_m^{\dagger}(k) = \frac{e^{\dagger}(k) + e^{\dagger}(k-1)}{2}, \tag{8}$$

$$v_m^{\dagger}(k) = \frac{v^{\dagger}(k) + v^{\dagger}(k-1)}{2}, \tag{9}$$

and $\Delta e^{\dagger}(k)$ is the backward difference of sequence $e^{\dagger}(k)$, that is,

$$\Delta e^{\dagger}(k) = e^{\dagger}(k) - e^{\dagger}(k-1). \tag{10}$$

The relationship between equations (6) and (7) with respect to the continuous values is shown by the block diagram in Fig. 3. In this figure, δ is defined as

$$\delta(z) := \frac{2}{h} \cdot \frac{1 - z^{-1}}{1 + z^{-1}}. \tag{11}$$

Thus, the loop transfer function from v^* to e^* can be given by $W(\beta, q, z)$, as shown in Fig. 4, where

$$W(\beta, q, z) = \frac{(1 + q\delta(z))G(z)C(z)}{1 + (K + \beta q\delta(z))G(z)C(z)}, \tag{12}$$

and r', d' are transformed exogenous inputs. Here, the variables such as v^*, u' and y' written in Fig. 4 indicate the z-transformed ones.
In this study, the following assumption is provided on the basis of the relatively fast sampling and the slow response of the controlled system.

[Assumption] The absolute value of the backward difference of sequence $e(k)$ does not exceed γ, i.e.,

$$|\Delta e(k)| = |e(k) - e(k-1)| \leq \gamma. \tag{13}$$

If condition (13) is satisfied, $\Delta e^{\dagger}(k)$ is exactly $\pm\gamma$ or 0 because of the discretization. That is, the absolute value of the backward difference can be given as

$$|\Delta e^{\dagger}(k)| = |e^{\dagger}(k) - e^{\dagger}(k-1)| = \gamma \text{ or } 0. \quad \square$$

The assumption stated above will be satisfied by the following examples. The phase trace of backward difference $\Delta e^{\dagger}$ is shown in the figures.

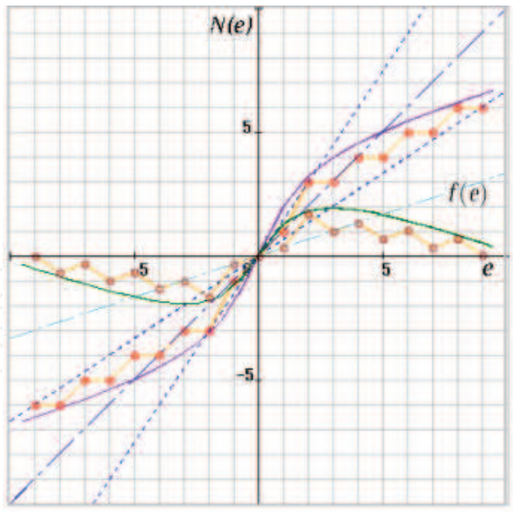

Fig. 5. Nonlinear characteristics and discretized outputs.

4. Norm inequalities

In this section, some lemmas with respect to an ℓ_2 norm of the sequences are presented. Here, we define a new nonlinear function

$$f(e) := g(e) + \beta\, e. \tag{14}$$

When considering the discretized output of the nonlinear characteristic, $v^\dagger = g(e^\dagger)$, the following expression can be given:

$$f(e^\dagger(k)) = v^\dagger(k) + \beta e^\dagger(k). \tag{15}$$

From inequality (4), it can be seen that the function (15) belongs to the first and third quadrants. Figure 5 shows an example of the continuous nonlinear characteristics $u = N(e)$ and $f(e)$, the discretized outputs $u^\dagger = N_d(e^\dagger)$ and $f(e^\dagger)$, and the sector (4) to be considered. When considering the equivalent linear characteristic, the following inequality can be defined:

$$0 \le \psi(k) := \frac{f(e^\dagger(k))}{e^\dagger(k)} \le 2\beta. \tag{16}$$

When this type of nonlinearity $\psi(k)$ is used, inequality (4) can be expressed as

$$v^\dagger(k) = g(e^\dagger(k)) = (\psi(k) - \beta)e^\dagger(k). \tag{17}$$

For the neutral points of $e^\dagger(k)$ and $v^\dagger(k)$, the following expression is given from (15):

$$\frac{1}{2}(f(e^\dagger(k)) + f(e^\dagger(k-1))) = v_m^\dagger(k) + \beta e_m^\dagger(k). \tag{18}$$

Moreover, equation (17) is rewritten as $v_m^\dagger(k) = (\psi(k) - \beta)e_m^\dagger(k)$. Since $|e_m^\dagger(k)| \le |e_m(k)|$, the following inequality is satisfied when a round-down discretization is executed:

$$|v_m^\dagger(k)| \le \beta|e_m^\dagger(k)| \le \beta|e_m(k)|. \tag{19}$$

Based on the above premise, the following norm conditions are examined

[Lemma-1] The following inequality holds for a positive integer p:

$$\|v_m^\dagger(k)\|_{2,p} \leq \beta \|e_m^\dagger(k)\|_{2,p} \leq \beta \|e_m(k)\|_{2,p}. \tag{20}$$

Here, $\|\cdot\|_{2,p}$ denotes the Euclidean norm, which can be defined by

$$\|x(k)\|_{2,p} := \left(\sum_{k=1}^{p} x^2(k) \right)^{1/2}.$$

(Proof) The proof is clear from inequality (19). □

[Lemma-2] If the following inequality is satisfied with respect to the inner product of the neutral points of (15) and the backward difference:

$$\langle\, v_m^\dagger(k) + \beta e_m^\dagger(k), \Delta e^\dagger(k) \,\rangle_p \geq 0, \tag{21}$$

the following inequality can be obtained:

$$\|v_m^{*\dagger}(k)\|_{2,p} \leq \beta \|e_m^{*\dagger}(k)\|_{2,p} \tag{22}$$

for any $q \geq 0$. Here, $\langle \cdot, \cdot \rangle_p$ denotes the inner product, which is defined as

$$\langle\, x_1(k), x_2(k) \,\rangle_p = \sum_{k=1}^{p} x_1(k) x_2(k).$$

(Proof) The following equation is obtained from (6) and (7):

$$\beta^2 \|e_m^{*\dagger}(k)\|_{2,p}^2 - \|v_m^{*\dagger}(k)\|_{2,p}^2 = \beta^2 \|e_m^\dagger(k)\|_{2,p}^2 - \|v_m^\dagger(k)\|_{2,p}^2 + \frac{2\beta q}{h} \cdot \langle v_m^\dagger(k) + \beta e_m^\dagger(k), \Delta e^\dagger(k) \rangle_p. \tag{23}$$

Thus, (22) is satisfied by using the left inequality of (20). Moreover, as for the input of $g^*(\cdot)$, the following inequality can be obtained from (23) and the right inequality (20):

$$\|v_m^{*\dagger}(k)\|_{2,p} \leq \beta \|e_m^*(k)\|_{2,p}. \tag{24}$$

□

The left side of inequality (21) can be expressed as a sum of trapezoidal areas.

[Lemma-3] For any step p, the following equation is satisfied:

$$\sigma(p) := \langle\, v_m^\dagger(k) + \beta e_m^\dagger(k), \Delta e^\dagger(k) \,\rangle_p = \frac{1}{2} \sum_{k=1}^{p} (f(e^\dagger(k)) + f(e^\dagger(k-1))) \Delta e^\dagger(k). \tag{25}$$

(Proof) The proof is clear from (18). □

In order to understand easily, an example of the sequences of continuous/discretized signals and the sum of trapezoidal areas is depicted in Fig. 6. The curve e and the sequence of circles $e^\dagger$ show the input of the nonlinear element and its discretized signal. The curve u and the sequence of circles $u^\dagger$ show the corresponding output of the nonlinear characteristic and its discretized signal, respectively. As is shown in the figure, the sequences of circles $e^\dagger$ and $u^\dagger$ trace on a grid pattern that is composed of integers. The sequence of circles $v^\dagger$ shows

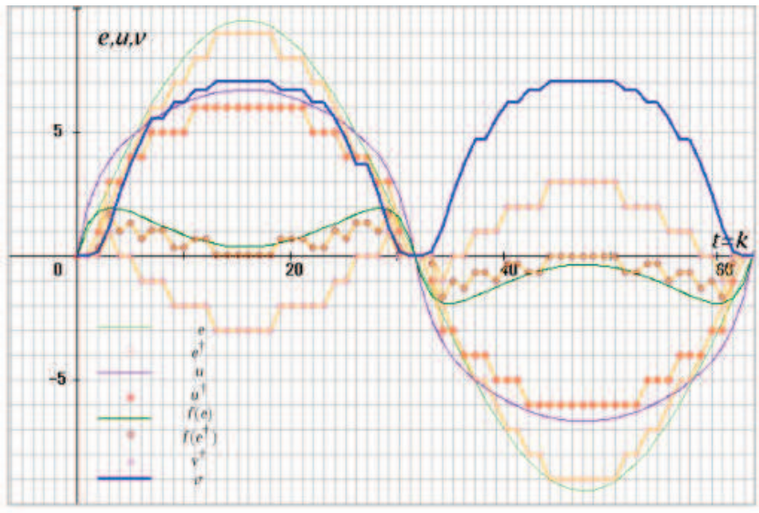

Fig. 6. Discretized input/output signals of a nonlinear element.

the discretized output of the nonlinear characteristic $g(\cdot)$. The curve of shifted nonlinear characteristic $f(e)$ and the sequence of circles $f(e^{\dagger})$ are also shown in the figure.
In general, the sum of trapezoidal areas holds the following property.

[Lemma-4] If inequality (13) is satisfied with respect to the discretization of the control system, the sum of trapezoidal areas becomes non-negative for any p, that is,

$$\sigma(p) \geq 0. \tag{26}$$

(Proof) Since $f(e^{\dagger}(k))$ belongs to the first and third quadrants, the area of each trapezoid

$$\tau(k) := \frac{1}{2}(f(e^{\dagger}(k)) + f(e^{\dagger}(k-1)))\Delta e^{\dagger}(k) \tag{27}$$

On the other hand, the trapezoidal area $\tau(k)$ is non-positive when $e(k)$ decreases (increases) in the first (third) quadrant. Strictly speaking, when ($e(k) \geq 0$ and $\Delta e(k) \geq 0$) or ($e(k) \leq 0$ and $\Delta e(k) \leq 0$), $\tau(k)$ is non-negative for any k. On the other hand, when ($e(k) \geq 0$ and $\Delta e(k) \leq 0$) or ($e(k) \leq 0$ and $\Delta e(k) \geq 0$), $\tau(k)$ is non-positive for any k. Here, $\Delta e(k) \geq 0$ corresponds to $\Delta e^{\dagger}(k) = \gamma$ or 0 (and $\Delta e(k) \leq 0$ corresponds to $\Delta e^{\dagger}(k) = -\gamma$ or 0) for the discretized signal, when inequality (13) is satisfied.
The sum of trapezoidal area is given from (25) as:

$$\sigma(p) = \sum_{k=1}^{p} \tau(k). \tag{28}$$

Therefore, the following result is derived based on the above. The sum of trapezoidal areas becomes non-negative, $\sigma(p) \geq 0$, regardless of whether $e(k)$ (and $e^{\dagger}$(k)) increases or decreases. Since the discretized output traces the same points on the stepwise nonlinear characteristic, the sum of trapezoidal areas is canceled when $e(k)$ (and $e^{\dagger}(k)$ decreases (increases) from a certain point $(e^{\dagger}(k), f(e^{\dagger}(k)))$ in the first (third) quadrant. (Here, without loss of generality, the response of discretized point $(e^{\dagger}(k), f(e^{\dagger}(k)))$ is assumed to commence at the origin.) Thus, the proof is concluded. □

5. Robust stability in a global sense

By applying a small gain theorem to the loop transfer characteristic (12), the following robust stability condition of the discretized nonlinear control system can be derived

[Theorem] If there exists a $q \geq 0$ in which the sector parameter β with respect to nonlinear term $g(\cdot)$ satisfies the following inequality, the discrete-time control system with sector nonlinearity (4) is robust stable in an ℓ_2 sense:

$$\beta < \beta_0 = K \cdot \eta(q_0, \omega_0) = \max_q \min_\omega K \cdot \eta(q, \omega), \tag{29}$$

when the linearized system with nominal gain K is stable.
The η-function is written as follows:

$$\eta(q, \omega) := \frac{-q\Omega \sin\theta + \sqrt{q^2\Omega^2 \sin^2\theta + \rho^2 + 2\rho\cos\theta + 1}}{\rho}, \quad \forall \omega \in [0, \omega_c], \tag{30}$$

where $\Omega(\omega)$ is the distorted frequency of angular frequency ω and is given by

$$\delta(\mathrm{e}^{j\omega h}) = j\Omega(\omega) = j\frac{2}{h}\tan\left(\frac{\omega h}{2}\right), \quad j = \sqrt{-1} \tag{31}$$

and ω_c is a cut-off frequency. In addition, $\rho(\omega)$ and $\theta(\omega)$ are the absolute value and the phase angle of $KG(\mathrm{e}^{j\omega h})C(\mathrm{e}^{j\omega h})$, respectively.
(Proof) Based on the loop characteristic in Fig. 4, the following inequality can be given with respect to $z = \mathrm{e}^{j\omega h}$:

$$\|e_m^*(z)\|_{2,p} \leq c_1\|r_m'(z)\|_{2,p} + c_2\|d_m'(z)\|_{2,p} + \sup_{z=1}|W(\beta, q, z)| \cdot \|w_m^{*\dagger}(z)\|_{2,p}. \tag{32}$$

Here, $r_m'(z)$ and $d_m'(z)$ denote the z-transformation for the neutral points of sequences $r'(k)$ and $d'(k)$, respectively. Moreover, c_1 and c_2 are positive constants.
By applying inequality (24), the following expression is obtained:

$$\left(1 - \beta \cdot \sup_{z=1}|W(\beta, q, z)|\right)\|e_m^*(z)\|_{2,p} \leq c_1\|r_m'(z)\|_{2,p} + c_2\|d_m'(z)\|_{2,p}. \tag{33}$$

Therefore, if the following inequality (i.e., the small gain theorem with respect to ℓ_2 gains) is valid,

$$|W(\beta, q, \mathrm{e}^{j\omega h})| = \left|\frac{(1 + jq\Omega(\omega))P(\mathrm{e}^{j\omega h})C(\mathrm{e}^{j\omega h})}{1 + (K + j\beta q\Omega(\omega))P(\mathrm{e}^{j\omega h})C(\mathrm{e}^{j\omega h})}\right| = \left|\frac{(1 + jq\Omega(\omega))\rho(\omega)\mathrm{e}^{j\theta(\omega)}}{K + (K + j\beta q\Omega(\omega))\rho(\omega)\mathrm{e}^{j\theta(\omega)}}\right| < \frac{1}{\beta}. \tag{34}$$

the sequences $e_m^*(k)$, $e_m(k)$, $e(k)$ and $y(k)$ in the feedback system are restricted in finite values when exogenous inputs $r(k)$, $d(k)$ are finite and $p \to \infty$. (The definition of ℓ_2 stable for discrete-time systems was given in (10; 11).)
From the square of both sides of inequality (34),

$$\beta^2\rho^2(1 + q^2\Omega^2) < (K + K\rho\cos\theta - \beta\rho q\Omega\sin\theta)^2 + (K\rho\sin\theta + \beta\rho q\Omega\cos\theta)^2.$$

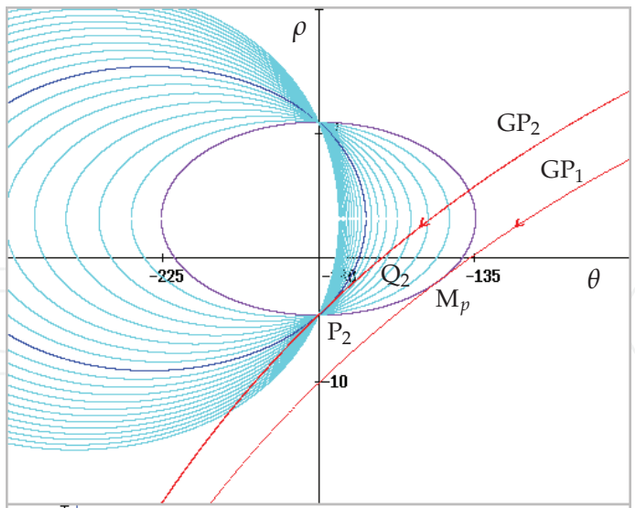

Fig. 7. An example of modified Nichols diagram $(M = 1.4,\ c_q = 0.0, 0.2, \cdots, 4.0)$.

Thus, the following quadratic inequality can be obtained:

$$\beta^2\rho^2 < -2\beta K\rho q\Omega \sin\theta + K^2(1+\rho\cos\theta)^2 + K^2\rho^2\sin^2\theta. \tag{35}$$

Consequently, as a solution of inequality (35),

$$\beta < \frac{-Kq\Omega\sin\theta + K\sqrt{q^2\Omega^2\sin^2\theta + \rho^2 + 2\rho\cos\theta + 1}}{\rho} = K\eta(q,\omega). \tag{36}$$

□

6. Modified Nichols diagram

In the previous papers,the inverse function was used instead of the η-function, i.e.,

$$\xi(q,\omega) = \frac{1}{\eta(q,\omega)}.$$

Using the notation, inequality (29) can be rewritten as follows:

$$M_0 = \xi(q_0,\omega_0) = \min_q \max_\omega \xi(q,\omega) < \frac{K}{\beta}. \tag{37}$$

When $q = 0$, the ξ-function can be expressed as:

$$\xi(0,\omega) = \frac{\rho}{\sqrt{\rho^2 + 2\rho\cos\theta + 1}} = |T(\mathrm{e}^{j\omega h})|, \tag{38}$$

where $T(z)$ is the complementary sensitivity function for the discrete-time system.
It is evident that the following curve on the gain-phase plane,

$$\xi(0,\omega) = M, \quad (M : \text{const.}) \tag{39}$$

corresponds to the contour of the constant M in the Nichols diagram. In this study, since an arbitrary non-negative number q is considered, the ξ-function that corresponds to (38) and (39) is given as follows:

$$\frac{\rho}{-q\Omega\sin\theta+\sqrt{q^2\Omega^2\sin^2\theta+\rho^2+2\rho\cos\theta+1}}=M. \tag{40}$$

From this expression, the following quadratic equation can be obtained:

$$(M^2-1)\rho^2+2\rho M(M\cos\theta-q\Omega\sin\theta)+M^2=0. \tag{41}$$

The solution of this equation is expressed as follows:

$$\rho=-\frac{M}{M^2-1}(M\cos\theta-q\Omega\sin\theta)\pm\frac{M}{M^2-1}\sqrt{(M\cos\theta-q\Omega\sin\theta)^2-(M^2-1)}. \tag{42}$$

The modified contour in the gain-phase plane (θ, ρ) is drawn based on the equation of (42). Although the distorted frequency Ω is a function of ω, the term $q\Omega=c_q\geq 0$ is assumed to be a constant parameter. This assumption for M contours was also discussed in (11). Figure 7 shows an example of the modified Nichols diagram for $c_q\geq 0$ and $M=1.4$. Here, GP_1 is a gain-phase curve that touches an M contour at the peak value ($M_p=\xi(0,\omega_p)=1.4$). On the other hand, GP_2 is a gain-phase curve that crosses the $\theta=-180^\circ$ line and all the M contours at the gain crossover point P_2. That is, the gain margin g_M becomes equal to $-20\log_{10}M/(M+1)=4.68$[dB]. The latter case corresponds to the discrete-time system in which Aizerman's conjecture is valid (14; 15). At the continuous saddle point P_2, the following equation is satisfied:

$$\left(\frac{\partial\xi(q,\omega)}{\partial q}\right)_{q=q_0,\omega=\omega_0}=0. \tag{43}$$

Evidently, the phase margin p_M is obtained from the phase crossover point Q_2.

7. Controller design

The PID controller applied in this study is given by the following algorithm:

$$u_c(k)=K_pu^\dagger(k)+C_i\sum_{j=0}^{k}u^\dagger(j)+C_d\Delta u^\dagger(k), \tag{44}$$

where $\Delta u^\dagger(k)=u^\dagger(k)-u^\dagger(k-1)$ is a backward difference in integer numbers, and each coefficient is defined as

$$K_p,\ C_i,\ C_d\in Z_+,\quad Z_+=\{0,1,2,3\cdots\}.$$

Here, K_p, C_i, and C_d correspond to K_p, K_ph/T_I, and K_pT_D/h in the following (discrete-time z-transform expression) PID algorithm:

$$C(z)=K_p\left(1+\frac{h}{T_I(1-z^{-1})}+\frac{T_D}{h}(1-z^{-1})\right). \tag{45}$$

We use algorithm (44) without division because the variables $u^\dagger$, u_c, and coefficients K_p, C_i, C_d are integers.

Using the z-transform expression, equation (44) is written as:

$$\begin{aligned} u_c(z) &= C(z)u(z) \\ &= \left(K_p + C_i(1 + z^{-1} + z^{-2} + \cdots) + C_d(1 - z^{-1})\right) u(z). \end{aligned}$$

In the closed form, controller $C(z)$ can be given as

$$C(z) = K_p + C_i \cdot \frac{1}{1 - z^{-1}} + C_d(1 - z^{-1}) \tag{46}$$

for discrete-time systems. When comparing equations (45) and (46), C_i and C_d become equal to $K_p h/T_I$ and $K_p T_D/h$, respectively.
The design method adopted in this paper is based on the classical parameter specifications in the modified Nichols diagram. This method can be conveniently designed, and it is significant in a physical sense (i.e., mechanical vibration and resonance).
Furthermore, in this article, PID-D^2 is considered. The algorithm is written as

$$u_c(k) = K_p u^{\dagger}(k) + C_i \sum_{j=0}^{k} u^{\dagger}(j) + C_{d1}\Delta u^{\dagger}(k) + C_{d2}\Delta^2 u^{\dagger}(k), \tag{47}$$

where

$$\Delta^2 u^{\dagger}(k) = \Delta u^{\dagger}(k) - \Delta u^{\dagger}(k-1) = u^{\dagger}(k) - 2u^{\dagger}(k-1) + u^{\dagger}(k-2).$$

Thus, the controller $C(z)$ can be given as

$$C(z) = K_p + C_i \cdot \frac{1}{1 - z^{-1}} + C_{d1}(1 - z^{-1}) + C_{d2}(1 - 2z^{-1} + z^{-2}) \tag{48}$$

for discrete-time systems.

8. Numerical examples

[Example-1] Consider the following third order controlled system:

$$G(s) = \frac{K_1}{(s + 0.04)(s + 0.2)(s + 0.4)}, \tag{49}$$

where $K_1 = 0.0002 = 2.0 \times 10^{-4}$.

	K_p	C_i	C_d	β_0	g_M[dB]	p_M[deg]	M_p
(i)	100	0	0	β	7.72	34.9	1.82
(ii)	100	3	0	0.98	5.92	23.8	2.61
(iii)	100	3	120	β	11.1	35.4	1.69
(iv)	50	0	0	β	10.8	48.6	1.29
(v)	50	2	0	1.00	7.92	30.6	1.99
(vi)	50	2	60	β	13.3	40.5	1.45

Table 1. PID parameters for Example-1 (g_M: gain margins, p_M: phase margins, M_p: peak values, β_0: allowable sectors).

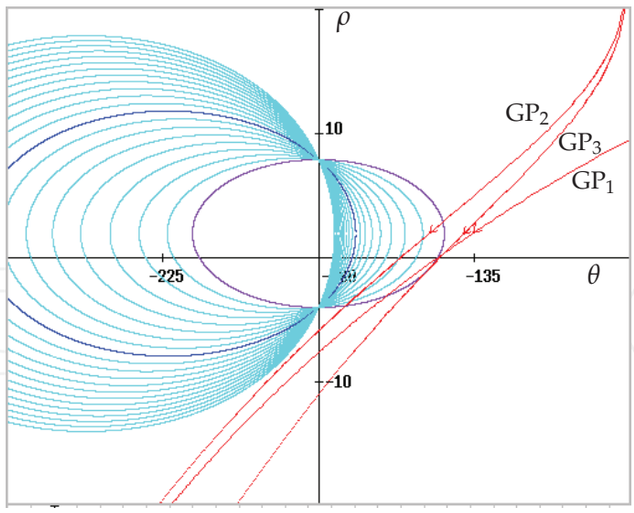

Fig. 8. Modified contours and gain-phase curves for Example-1 ($M = 1.69$, $c_q = 0.0, 0.2, \cdots, 4.0$).

The discretized nonlinear characteristic (discretized sigmoid, i.e. arc tangent (12)) is as shown in Fig. **??** (a). In this article, the resolution value and the sampling period are assumed to be $\gamma = 1.0$ and $h = 1.0$ as described in section 2.
When choosing the nominal gain $K = 1.0$ and the threshold $\varepsilon = 2.0$, the sectorial area of the discretized nonlinear characteristic for $\varepsilon \leq |e|$ can be determined as [0.5, 1.5] drawn by dotted lines in the figure. Figure 8 shows gain-phase curves of $KG(\mathrm{e}^{j\omega h})C(\mathrm{e}^{j\omega h})$ on the modified Nichols diagram. Here, GP_1, GP_2, and GP_3 are cases (i), (ii), and (iii), respectively. The PID parameters are specified as shown in Table 1. The gain margins g_M, the phase margin p_M and the peak value M_p can be obtained from the gain crossover points P, the phase crossover points Q, and the points of contact with regard to the M contours, respectively.
The max-min value β_0 is calculated from (29) (e.g., (ii)) as follows:

$$\beta_0 = \max_q \min_\omega \; K \cdot \eta(q, \omega) = K \cdot \eta(q_0, \omega_0) = 0.98.$$

Therefore, the allowable sector for nonlinear characteristic $g(\cdot)$ is given as [0.0, 1.98]. The stability of discretized control system (ii) (and also systems (i),(iii)) will be guaranteed. In this example, the continuous saddle point (43) appears (i.e., Aizerman's conjecture is satisfied). Thus, the allowable interval of equivalent linear gain K_ℓ can be given as $0 < K_\ell < 1.98$. In the case of (i) and (iii), β_0 becomes not less than K. However, from the definition of (4), $\bar{\beta}$ in the tables should be considered $\beta_0 = \bar{\beta} = 1.0$. Figure 9 shows step responses for the three cases. In this figure, the time-scale line is drawn in $10h$ increments because of avoiding indistinctness.
Sequences of the input $u^\dagger(k)$ and the output $u_c^\dagger$ of PID controller are also shown in the figure. Here, $u_c^\dagger(k)$ is drawn to the scale of $1/100$. Figure 10 shows phase traces (i.e., sequences of $(e(k), \Delta e(k))$ and $(e^\dagger((k), \Delta e^\dagger(k)))$. As is obvious from Fig. 10, assumtion (13) is satisfied. The step response (i) remains a sutained oscillation and an off-set. However, as for (ii) and (iii) the responses are improved by using the PID, especially integral (I: a summation in this paper) algorithm.
The discretized linear characteristic as shown in Fig. **??** (b) is also considered here. In the figure, the sectorial area of the discretized characteristic for $\varepsilon \leq |e|$ can be determined as [0.5, 0.85] drawn by dotted lines, and the nominal gain is given as $K = 0.675$. When

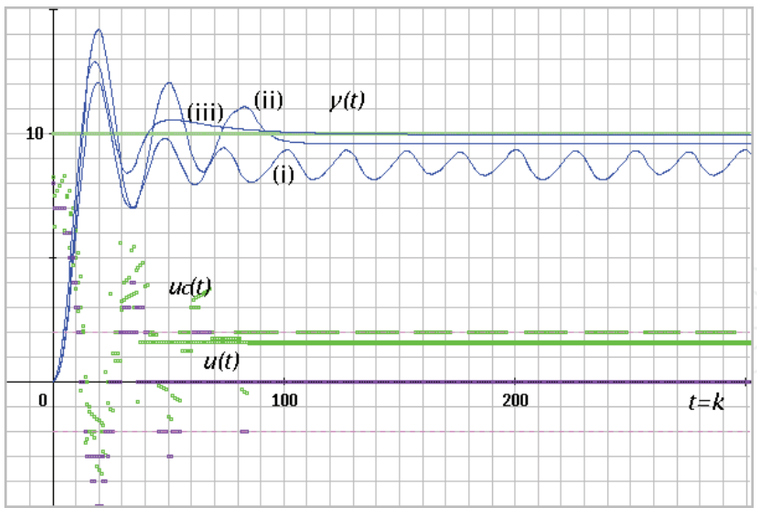

Fig. 9. Step responses for Example-1.

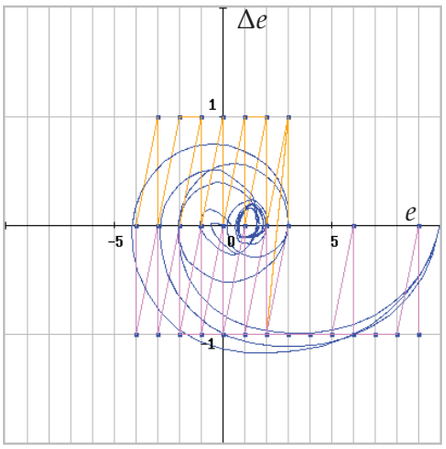

Fig. 10. Phase traces for Example-1.

normalizing the nominal gain for $K = 1.0$ (i.e., choosing the gain constant $K_2 = K_1/0.675$), the sectorial area is determined as [0.74, 1.26]. In this case, an example of step responces is depicted in Fig. 11. The PID parameters used here are also shown in Table 1.

[Example-2] Consider the following fourth order controlled system:

$$G(s) = \frac{K_1}{(s+0.04)(s+0.2)(s+0.4)(s+1.0)}, \tag{50}$$

where $K_1 = 0.0002 = 2.0 \times 10^{-4}$. The same nonlinear characteristic and the nominal gain are chosen as shown in Example-1.
Figure 12 shows gain-phase curves of $KG(e^{j\omega h})C(e^{j\omega h})$ on the modified Nichols diagram. Here, GP_1, GP_2, GP_3 and GP_4 are cases (i), (ii), (iii) and (iv) in Table 2, respectively. In this example, PID-D^2 control scheme is also used. The PID-D^2 parameters are specified as shown

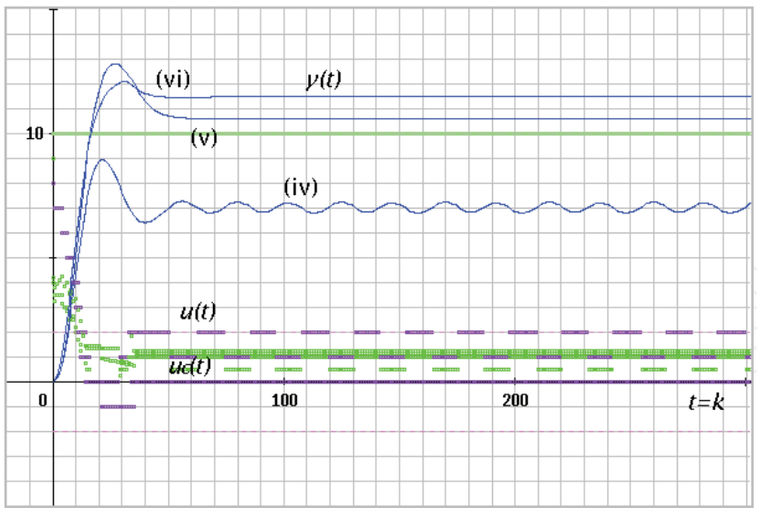

Fig. 11. Step responses for Example-1 (Discretized linear case).

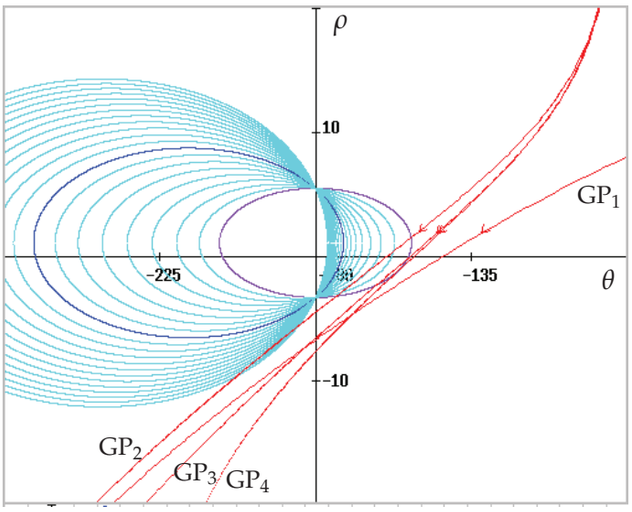

Fig. 12. Modified contours and gain-phase curves for Example-2 ($M = 2.14$, $c_q = 0.0, 0.2, \cdots, 4.0$).

in the table. The max-min value β_0 is calculated from (29) (e.g., (iv)) as follows:

$$\beta_0 = \max_q \min_\omega K \cdot \eta(q, \omega) = K \cdot \eta(q_0, \omega_0) = 0.69.$$

Therefore, the allowable sector for nonlinear characteristic $g(\cdot)$ is given as [0.0, 1.69]. The stability of discretized control system (ii) (and also systems (i),(iii),(iv)) will be guaranteed. In this example, the continuous saddle point (43) appears (i.e., Aizerman's conjecture is satisfied). Thus, the allowable interval of equivalent gain K_ℓ can be given as $0 < K_\ell < 1.69$.

As is shown in Fig. 13, the step response (i) remains a sutained oscillation and an off-set. However, as for (ii), (iii) and (iv) the responses are improved by using PI, PID and PID-D^2 algorithm (D^2: a second difference).

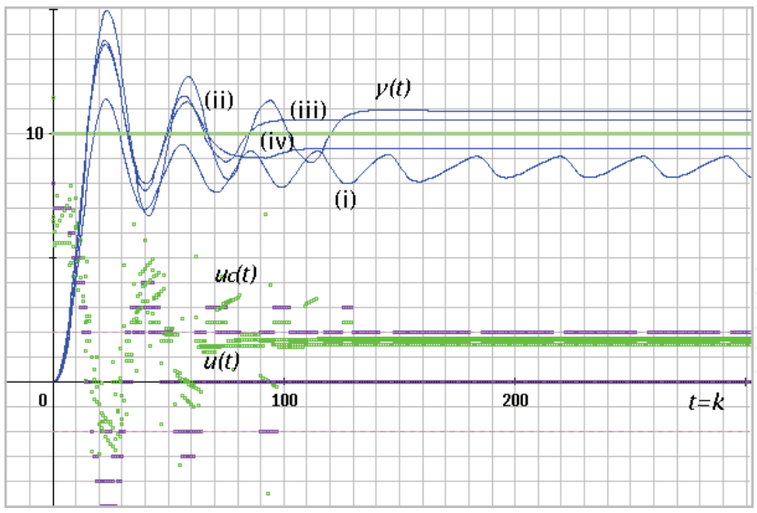

Fig. 13. Step responses for Example-2.

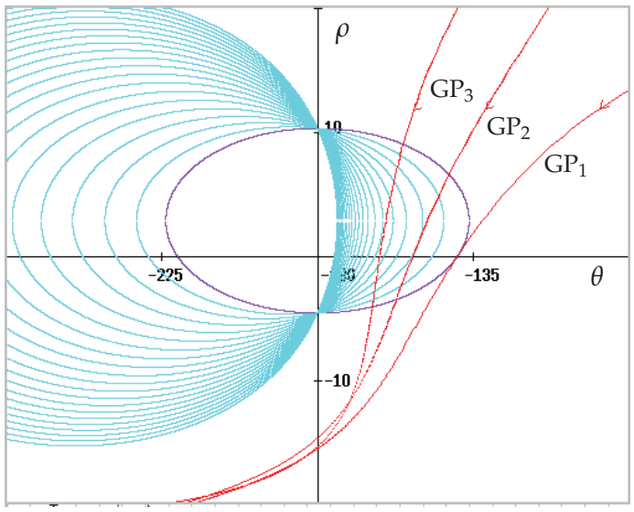

Fig. 14. Modified contours and gain-phase curves for Example-3 ($M = 1.44$, $c_q = 0.0, \cdots, 4.0$).

[Example-3] Consider the following nonminimum phase controlled system:

$$G(s) = \frac{K_2(s+0.2)(-s+0.4)}{(s+0.02)(s+0.04)(s+1.0)}, \tag{51}$$

	K_p	C_i	C_{d1}	C_{d2}	β_0	g_M[dB]	p_M[deg]	M_p
(i)	80	0	0	0	β	6.8	37.2	1.79
(ii)	80	3	0	0	0.69	4.69	20.9	3.10
(iii)	80	3	60	0	1.00	6.63	27.4	2.26
(iv)	80	3	60	120	β	7.76	28.8	2.14

Table 2. PID-D^2 parameters for Example-2.

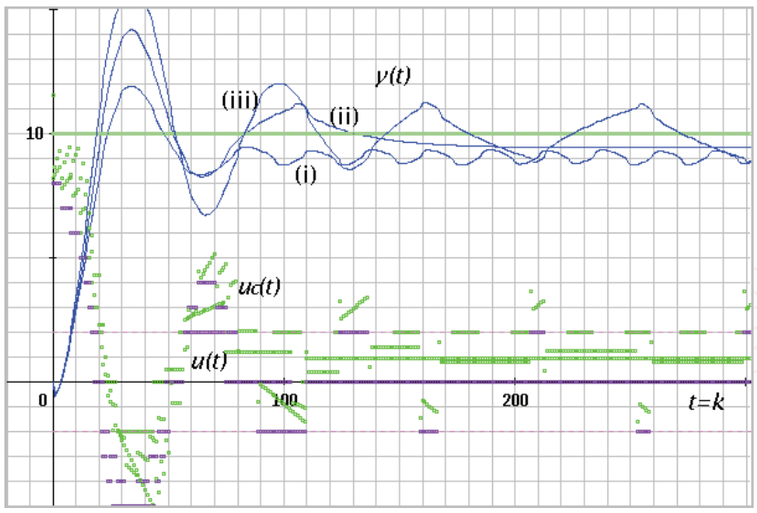

Fig. 15. Step responses for Example-3.

where $K_3 = 0.001 = 1.0 \times 10^{-3}$. Also, in this example, the same nonlinear characteristic and the nominal gain are chosen as shown in Example-1. The modified Nichols diagram with gain-phase curves of $KG(e^{j\omega h})C(e^{j\omega h})$ is as shown in Fig. 14. Here, GP_1, GP_2 and GP_3 are cases (i), (ii), and (iii), and the PID parameters are specified as shown in Table 3. Figure 15 shows time responses for the three cases.

For example, in the case of (iii), although the allowable sector of equivalent linear gain is $0 < K_\ell < 5.9$, the allowable sector for nonlinear characteristic becomes [0.0, 1.44] as shown in Table 3. Since the sectorial area of the discretized nonlinear characteristic is [0.5, 1.5], the stability of the nonlinear control system cannot be guaranteed. The response for (iii) actually fluctuates as shown in Figs. 15 and 16. This is a counter example for Aizerman's conjecture.

9. Conclusion

In this article, we have described robust stabilization and discretized PID control for continuous plants on a grid pattern with respect to controller variables and time elapsed. A robust stability condition for nonlinear discretized feedback systems was presented along with a method for designing PID control. The design procedure employs the modified Nichols diagram and its parameter specifications. The stability margins of the control system are specified directly in the diagram. Further, the numerical examples showed that the time responses can be stabilized for the required performance. The concept described in this article will be applicable to digital and discrete-event control system in general.

	K_p	C_i	C_d	β_0	g_M[dB]	p_M[deg]	M_p
(i)	100	0	0	0.92	15.5	40.6	1.44
(ii)	100	2	0	0.71	14.7	27.7	2.09
(iii)	100	4	40	0.44	15.3	18.1	3.18

Table 3. PID parameters for Example-3.

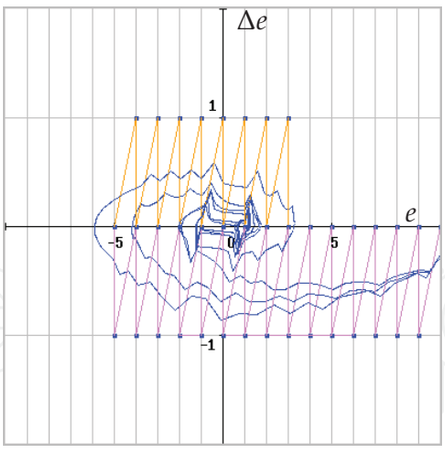

Fig. 16. Phase traces for Example-3.

10. References

[1] R. E. Kalman, "Nonlinear Aspects of Sampled-Data Control Systems", *Proc. of the Symposium on Nonlinear Circuit Analysis*, vol. VI, pp.273-313, 1956.

[2] R. E. Curry, *Estimation and Control with Quantized Measurements*, Cambridge, MIT Press, 1970.

[3] D. F. Delchamps, "Stabilizing a Linear System with Quantized State Feedback", *IEEE Trans. on Automatic Control*, vol. 35, pp. 916-924, 1990.

[4] M. Fu, "Robust Stabilization of Linear Uncertain Systems via Quantized Feedback", *Proc. of IEEE Int. Conf. on Decision and Control*, TuA06-5, 2003.

[5] A. Datta, M.T. Ho and S.P. Bhattacharyya, *Structure and Synthesis of PID Controllers*, Springer-Verlag, 2000.

[6] F. Takemori and Y. Okuyama, "Discrete-Time Model Reference Feedback and PID Control for Interval Plants" *Digital Control 2000:Past, Present and Future of PID Control*, Pergamon Press, pp. 260-265, 2000.

[7] Y. Okuyama, "Robust Stability Analysis for Discretized Nonlinear Control Systems in a Global Sense", *Proc. of the 2006 American Control Conference*, Minneapolis, USA, pp. 2321-2326, 2006.

[8] Y. Okuyama, "Robust Stabilization and PID Control for Nonlinear Discretized Systems on a Grid Pattern", *Proc. of the 2008 American Control Conference*, Seattle, USA, pp. 4746-4751, 2008.

[9] Y. Okuyama, "Discretized PID Control and Robust Stabilization for Continuous Plants", *Proc. of the 17th IFAC World Congress*, Seoul, Korea, pp. 1492-1498, 2008.

[10] Y. Okuyama *et al.*, "Robust Stability Evaluation for Sampled-Data Control Systems with a Sector Nonlinearity in a Gain-Phase Plane" *Int. J. of Robust and Nonlinear Control*, Vol. 9, No. 1, pp. 15-32, 1999.

[11] Y. Okuyama *et al.*, "Robust Stability Analysis for Non-Linear Sampled-Data Control Systems in a Frequency Domain", *European Journal of Control*, Vol. 8, No. 2, pp. 99-108, 2002.

[12] Y. Okuyama *et al.*, "Amplitude Dependent Analysis and Stabilization for Nonlinear Sampled-Data Control Systems", *Proc. of the 15th IFAC World Congress*, T-Tu-M08, 2002.

[13] Y. Okuyama, "Robust Stabilization and for Discretized PID Control Systems with Transmission Delay", *Proc. of IEEE Int. Conf. on Decision and Control*, Shanghai, P. R. China, pp. 5120-5126, 2009.
[14] L. T. Grujic, "On Absolute Stability and the Aizerman Conjecture", *Automatica*, pp. 335-349. 1981.
[15] Y. Okuyama *et al.*, "Robust Stability Analysis for Nonlinear Sampled-Data Control Systems and the Aizerman Conjecture", *Proc. of IEEE Int. Conf. on Decision and Control*, Tampa, USA, pp. 849-852, 1998.

Robust Control, Theory and Applications

Edited by Prof. Andrzej Bartoszewicz

ISBN 978-953-307-229-6
Hard cover, 678 pages
Publisher InTech
Published online 11, April, 2011
Published in print edition April, 2011

The main objective of this monograph is to present a broad range of well worked out, recent theoretical and application studies in the field of robust control system analysis and design. The contributions presented here include but are not limited to robust PID, H-infinity, sliding mode, fault tolerant, fuzzy and QFT based control systems. They advance the current progress in the field, and motivate and encourage new ideas and solutions in the robust control area.

InTech Europe
University Campus STeP Ri
Slavka Krautzeka 83/A
51000 Rijeka, Croatia
Phone: +385 (51) 770 447
Fax: +385 (51) 686 166
www.intechopen.com

InTech China
Unit 405, Office Block, Hotel Equatorial Shanghai
No.65, Yan An Road (West), Shanghai, 200040, China
中国上海市延安西路65号上海国际贵都大饭店办公楼405单元
Phone: +86-21-62489820
Fax: +86-21-62489821

IntechOpen